Appendix 4: Inference of ice cloud properties from high-spectral resolution infrared observations

Inference of ice cloud properties from high-spectral resolution infrared observations

Hung-Lung Huang[1], Ping Yang[2], Heli Wei[2], Bryan A. Baum[3,1], Yongxiang Hu[3],

Paolo Antonelli[1], Steven A. Ackerman[1]

[1] Cooperative Institute for Meteorological Satellite Studies, University of Wisconsin-Madison, 1225 W. Dayton Street, Madison, WI 53706

[2] **Texas A&M University, Department of Atmospheric Sciences, TX 77843**

[3] NASA Langley Research Center, Hampton, VA 23681

Corresponding author address: Dr. Ping Yang, Department of Atmospheric Sciences, Texas A&M University, TAMU 3150, College Station, TX 77843-3150. Tel: 979-845-4923; Fax: 979-862-4466; Email: pyang@ariel.met.tamu.edu

Abstract

The theoretical basis is explored for inferring the microphysical properties of ice crystal from high-spectral resolution infrared observations. A radiative transfer model is employed to simulate spectral radiances to address relevant issues. The extinction and absorption efficiencies of individual ice crystals, assumed as hexagonal columns for large particles and droxtals for small particles, are computed from a combination of the finite-difference time-domain (FDTD) technique and a composite method. The corresponding phase functions are computed from a combination of FDTD and an improved geometric optics method (IGOM). Bulk scattering properties are derived by averaging the single-scattering properties of individual particles for 30 particle size distributions developed from *in situ* measurements and for additional four analytical Gamma size distributions for small particles. The nonsphericity of ice crystals is shown to have a significant impact on the radiative signatures in the infrared (IR) spectrum; the spherical particle approximation for inferring ice cloud properties may result in an overestimation of the optical thickness and an inaccurate retrieval of effective particle size. Furthermore, we show that the error associated with the use of the Henyey-Greenstein phase function can be as larger as 1 K in terms of brightness temperature for larger particle effective size at some strong scattering wavenumbers. For small particles, the difference between the two phase functions is much less, with brightness temperatures generally differing by less than 0.4 K.

The simulations undertaken in this study show that the slope of the IR brightness temperature spectrum between 790–960 cm^{-1} is sensitive to the effective particle size. Furthermore, a strong sensitivity of IR brightness temperature to cloud optical thickness is noted within the 1050–1250 cm^{-1} region. Based on this spectral feature, a technique is presented for the simultaneous retrieval of the visible optical thickness and effective particle size from high spectral resolution infrared data under ice cloudy condition. The error analysis shows that the uncertainty of the retrieved optical thickness and effective particle size has a small range of variation. The error for retrieving particle size in conjunction with an uncertainty of 5 K in cloud temperature, or a surface temperature uncertainty of 2.5 K, is less than 15%. The corresponding error in the uncertainty of optical thickness is within 5-20%, depending on the value of cloud optical thickness. The applicability of the technique is demonstrated using the aircraft–based High-resolution Interferometer Sounder (HIS) data from the Subsonic Aircraft: Contrail and Cloud Effects Special Study (SUCCESS) in 1996 and the First ISCCP Regional Experiment - Arctic Clouds Experiment (FIRE-ACE) in 1998.

1. Introduction

Cirrus clouds play an important role in our climate system [1-4] yet their full impact on weather and climate change remains a puzzle. Substantial efforts have focused on remote sensing of cirrus clouds. Radiances observed by satellite-borne sensors at visible, near-infrared and mid-infrared wavelengths are widely used to retrieve cloud properties [5-9]. Emitted infrared radiation (IR), particularly in the atmospheric window region (i.e. 8-12 μm), contains a wealth of information on the properties of ice clouds. In the near future our ability to observe these global clouds will improve with the launch of new satellite instruments, such as the Geosynchronous Imaging Fourier Transform Spectrometer

(GIFTS) [10-11] and Cross-Track Infrared Sounder (CrIS) [12], that have high spectral resolution.

The high spectral resolution radiance spectrum contains some important information of cirrus clouds. The radiance at high spectral resolution over abroad wavelength range will lead improved cirrus clouds retrievals. High-resolution spectral signatures in the atmospheric window region have been used previously to study cloud and aerosol properties. Ou et al. [13] presented an algorithm to infer cirrus cloud properties from Airborne Remote Earth Sensing system (ARES) data within two mid-IR atmospheric window (5.1-5.3 μm and 3.7 μm) bands. Various IR algorithms to infer ice cloud properties based on radiances within the 8-12 μm atmospheric window have been suggested (see references [14-16]). A number of these studies, such as *Chung et al.* [14] and *DeSlover et al.* [17], approximated ice particles as spheres for the determination of scattering properties. However, *Kahn et al.* [18] found that radiative transfer simulations performed with nonspherical ice particle scattering models fit observed transmission spectra more accurately than simulations based on the spherical approximation employed in light scattering computation. A similar conclusion was reached by *Eldering et al.* [19] who used high-resolution spectra of non-gas-absorption transmission from Atmospheric Trace Molecule Spectroscopy Experiment (ATMOS) sun occultation data for cirrus cloud identification. *Rathke and Fischer* [20] presented an algorithm for inferring water cloud microphysical properties from high-resolution IR spectra, and investigated the sensitivity of the retrievals for clouds of moderate optical thickness.

The intent of the present study is to explore an approach for simultaneously retrieving cirrus cloud microphysical properties from the aircraft-based interferometer measurements in the 750–1250 cm^{-1} (i.e. 8-13.3 μm) spectral region. The present algorithm developed for retrieving cloud properties is complementary to the approaches based on the visible and near-IR spectral signatures reported by Nakajima and King [5], King et al. [6] and Platnick et al. [7].

This paper proceeds as follows. Section 2 presents the methodology for deriving the single-scattering properties of ice crystals and the numerical model for IR radiative transfer. This section also discusses the effect of ice crystal non-sphericity and the Henyey-Greenstein (H-G) phase function assumption on the radiative properties of ice crystals in the IR atmospheric window region. Section 3 presents the theoretical basis for inferring the microphysical and optical properties of ice clouds. Various sensitivity studies are carried out to understand the sensitivity of simulated brightness temperatures to the optical thickness and particle effective size of ice clouds. An error analysis for our algorithm is also presented in Section 3 where various factors that affect the retrieval accuracy are discussed. Shown in Section 4 are two example cases for the simultaneous retrieval of the ice cloud effective particle size and optical thickness that were observed during the SUCCESS in 1996 and the FIRE-ACE in 1998. Finally, the study is summarized in Section 6.

2. Single Scattering Properties of Ice Clouds and Radiative Transfer Simulations

To infer cloud properties from satellite- or aircraft-borne measurements using IR interferometer data, the radiance measurements are compared to theoretical simulations using a radiative transfer model (including a single-scattering module) that we describe in this section.

2.1 Single-scattering Properties of Ice /Cirrus Clouds

Scattering by ice crystals in the IR spectral region is non-negligible [21]. Although various *in- situ* observations have demonstrated that ice clouds are almost exclusively composed of nonspherical ice crystals (e.g. [22-23]), studies involving IR radiance measurements often assume ice particles to be spherical. Simulation studies by *Chung et al.* [14] found that the assumption of a spherical geometry for ice crystals may be adequate for very small ice crystals at IR wavelengths.

Heymsfield and Iaquinta [23] showed that in the upper portions of cirrus clouds, where the temperatures tend to be cold, the ice particles are small. Although these small particles are nonspherical, they tend to have aspect ratios (the ratio of particle length to its width) close to unity. *Yang et al.* [24] suggested the shape of small ice crystals may be represented by the droxtal geometry. *In-situ* measurements from the First ISCCP (International Satellite Cloud Climatology Project) Regional Experiment-II (FIRE-II) held in Coffeyville, Kansas in 1991, have shown that the middle to upper layers of midlatitude cirrus clouds are often composed of droxtals and pristine hexagonal crystals (see Fig. 15 of reference [23]). This is an important observation since the upwelling radiance in the IR spectral region tends to be dominated by absorption and scattering from the middle to upper regions of the cloud.

In this study, we use droxtals to represent small particles with size up to 32 μm in terms of maximum dimension, and hexagonal columns to represent larger particles. A number of investigators assume that ice crystals are hexagonal, which is a traditional non-spherical particle. Yang et al. [25] explained the use of hexagonal ice crystals for radiative transport through cirrus clouds.

Scattering and absorption properties of droxtals and small hexagonal ice crystals are calculated using the finite-difference time-domain (FDTD) method [26]. Figure 1 shows a comparison of the scattering phase functions at 1250 cm^{-1} for spherical, droxtal and hexagonal (with an aspect ratio of 1) ice crystal particles with the same maximum dimension of 10 μm. The phase function of the spherical particle was calculated from Lorenz-Mie theory using the computation code developed by *Wiscombe* [27]. As shown in Fig. 1, the scattering phase function is different for the three particle geometries in forward and backward directions. The forward scattering by droxtals is smaller than that by either hexagonal or spherical crystals because the volume of the droxtal is the smallest for the same maximum dimension. The positions of scattering sub-maximum are different for different shapes.

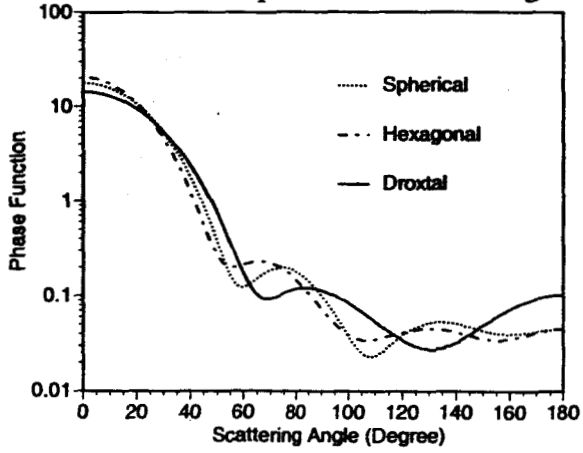

Figure 1. Comparison of phase functions for droxtals, hexagonal columns, and spherical ice crystals with maximum dimension 10 μm at a wavenumber of 1250 cm^{-1} (wavelength 8.0 μm).

The extinction and absorption efficiencies for crystals ranging from 35 to 10,000 μm in size are derived on the basis of the composite approach reported in Fu et al. [28]. This approach uses FDTD or other accurate method to calculate the single-scattering properties for small particles, and the weighted summation of approximate methods (such as geometric optics method (GOM) and equivalent Mie theory) to calculate the single-scattering properties for moderate to large particles. The corresponding phase functions for larger particle sizes are derived from an improved geometric optics (IGOM) [29]. We noticed that the difference between the phase function computed from IGOM and that from an asymptotic solution [30] are quit similar for the spectral region involved in this study, if the size of the crystal are larger than approximately 40 μm. A recent study by Lee et al. [31] has confirmed the applicability of the IGOM for IR phase function computations in the case of circular cylinders, as validated by the T-matrix [32] method in the case of circular cylinders.

The bulk ice cloud single-scattering properties are obtained by integrating the individual crystal scattering properties over 30 particle size distributions obtained during various campaigns for various ice clouds systems from Fu [33] and Mitchell et al[34]. Because no *in-situ* measurements are available for clouds at extremely low temperatures (expected to contain primarily small ice particles), we assume very cold clouds composed of small particles to follow Gamma analytical distributions with effective sizes of 6, 8, 10 and 12 μm. Fu and Sun [35] find that the retrieval of D_e is also sensitive to the ice particle size distribution assumed for ice crystal. The cirrus clouds at different geographic regions may have different size distributions due to differences in the thermodynamic and dynamic environments in which they form. This requires that a broad set of cirrus particle size distributions are needed in the retrieval process. The impact of the particle size distribution on the retrieval result deserves further study

The ice cloud bulk single-scattering properties are parameterized based on the effective particle size of the 34 size distributions. The effective size is defined as the 1.5 times of the ratio of average volume of ice crystal particles to their average projected area. Figure 2 shows the mean single-scattering properties (extinction efficiency, absorption efficiency, and asymmetry factor) for four effective sizes of ice clouds (D_e=10, 30, 50 and 80 μm) within the spectral range 750–1250 cm^{-1}. The calculations shown in Fig. 2 were performed using the parameterization scheme developed by *Yang et al.* [25] for the optical properties of ice crystals.

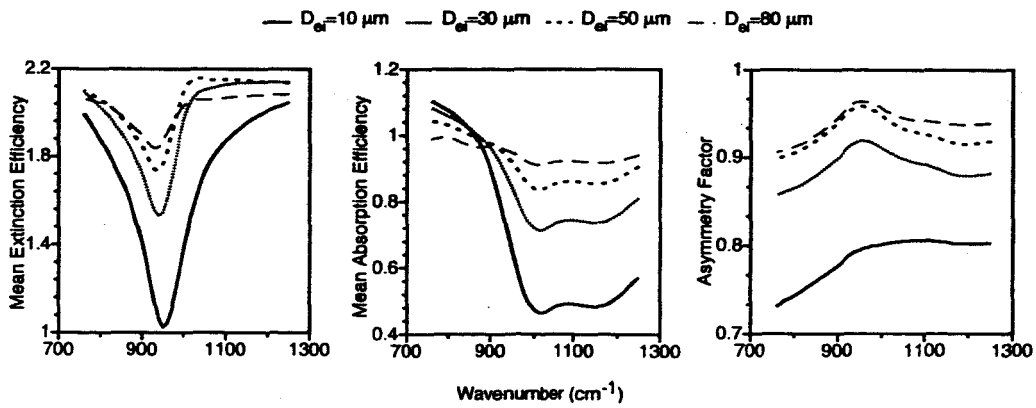

Figure 2. Single-scattering properties of ice clouds for four effective particle sizes

The mean extinction efficiency of ice crystals depends strongly on wavenumber, particularly, for small particle sizes. The extinction minimum at 950 cm^{-1}, which becomes more pronounced with decreasing particle size, corresponds to the Christiansen band of ice [36-37]. For large particle sizes (D_e=50 or 80 μm), the spectral variation of the extinction efficiency is relatively smooth. The total extinction efficiency of ice crystals (i.e., the sum of scattering and absorption effects) in the 1000–1250 cm^{-1} spectral region is nearly independent of effective particle size for large particles, a characteristic that is useful for the retrieval of ice cloud optical thickness.

The bulk absorption efficiency is related to the imaginary component of the refractive index of ice. In addition, the absorption of ice crystals depends on wavenumber and the effective particle size of the particles. The absorption efficiency varies with wavenumber in the 750–1000 cm^{-1} spectral region, particularly for small ice particles. This feature is useful for determining the effective size of ice crystals from high-resolution IR atmospheric spectral measurements. The asymmetry factor increases with effective particle size in the IR spectral region, implying that the scattering of the incident radiation by ice crystals is typically in the forward direction.

For water clouds, the bulk single scattering properties were calculated using the Lorenz-Mie theory [26], and assuming Gamma particle size distributions. The scattering properties of spherical particles have been extensively discussed by Hansen and Travis [38].

2.2 Numerical simulation of upwelling infrared radiances at aircraft level

Clear-sky (non-cloudy) monochromatic atmospheric molecular absorption optical thicknesses are computed from a line-by-line (LBL) radiative transfer model originally developed by Chou and Kouvaris [39]. For the present application, the atmosphere is divided into one hundred layers between the surface and an altitude of 20 km. Rawinsonde profiles provide atmospheric temperature, pressure, density and water vapor; the spectral line parameters of atmospheric gases are from HITRAN 2000 [40]; and the Voigt line shape [41] that accounts for both pressure and temperature broadening effects is used for computing the line absorption of atmospheric gas molecules. The continuum absorption of water vapor and other gases within 750–1250 cm^{-1} are calculated using the CKD-2.4 model [42]. To facilitate later comparisons with HIS data needed in the implementation of the retrieval technique, the monochromatic total optical thicknesses of atmospheric gases at every level are convolved with the instrumental response function. The upwelling atmospheric radiative spectrum under cloudy conditions at the aircraft altitude (20 km) is then computed in terms of brightness temperature by combining the clear-sky optical thickness from the LBL code and the discrete ordinates method radiative transfer (DISORT) [43]. Clouds are simulated by adding an optical thickness, single-scattering albedo, and scattering phase function into a model layer atmosphere. The DISORT method is used with 16 streams in calculations. The spectral interval is 0.2cm^{-1}. The Legendre extension coefficients of the phase function of ice crystals are derived using Hu's algorithm that properly accounts for the truncation of the strong forward peak [44].

2.3 Effect of Ice Crystal Nonsphericity

The significance of ice crystal nonsphericity in the retrieval of cloud optical thickness at visible and near infrared wavelengths has been discussed by Mishchenko et al. [45,46], Takano et al. [47] and references cited therein. Here we investigate the effect of ice

crystal nonsphericity on high-resolution IR spectral radiance simulations. Based on the single-scattering properties for same size distributions of both ice spheres and the hexagonal ice crystals, two sets of spectral-dependent brightness temperatures are calculated as functions of wavenumber. The visible optical thickness is fixed at 1 for these simulations. The two sets of resulting brightness temperatures for each size distribution are then differenced, with the results shown in Fig. 3 for the 800–1000 cm^{-1} spectral region. The brightness temperatures for spherical ice particles are 0.5–2.6 K lower than that for non-spherical particles. This is caused by the overestimation of the absorption and extinction efficiencies that occurs with the use of the spherical approximation [37].

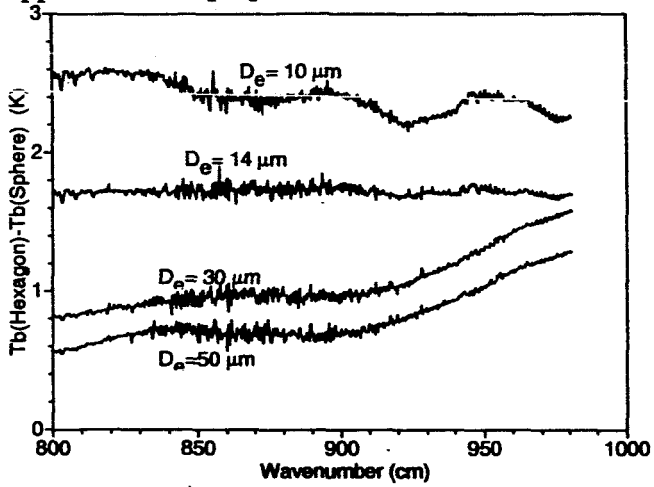

Figure 3. Shown are the differences in simulated upwelling brightness temperatures calculated for hexagonal ice crystals and spherical particles as a function of wavenumber for four effective sizes of ice clouds, but for a fixed cloud optical thickness of 1. Two sets of spectral brightness temperatures are calculated as a function of wavenumber based on the single-scattering properties for four particle size distributions of both ice spheres and the hexagonal ice crystals. The two sets of resulting brightness temperature spectra for each size distribution are then differenced. The atmospheric profiles are provided from a nearby rawinsonde. The surface skin temperature is 267.6 K and the cloud altitude is 7 km.

The previous results were obtained for a fixed optical thickness, but similar calculations can be made in which the particle size is fixed but the optical thickness varies. The results in Fig. 4 show the difference in spectral brightness temperatures calculated for three values of optical thickness within the 1100–1250 cm^{-1} spectral region, but for these simulations the effective particle size is fixed at 14 μm. The brightness temperatures for spherical ice particles are 1–2 K lower than that for non-spherical particles, depending on the optical thickness of the cloud.

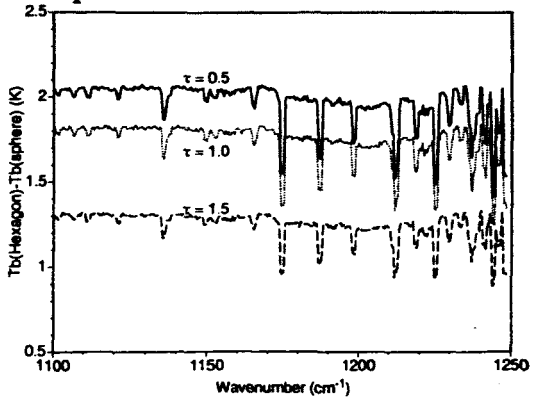

Figure 4. Shown are the differences in simulated upwelling brightness temperature spectra computed for hexagonal ice crystals and spherical particles. The brightness temperature differences are presented as a function of wavenumber for three cloud optical thicknesses. The effective particle size is fixed at 14 μm.

Figures 3 and 4 demonstrate that the nonsphericity of ice crystals can have a significant effect on the IR optical properties and that the spherical particle approximation for inferring ice cloud properties may result in an overestimation of the optical thickness and an inaccurate retrieval of effective particle size.

2.4 Errors caused by the use of the Henyey-Greenstein Phase Function

The impact of the nonspherical ice particles on optical properties raises the question of using a simplified form of the phase function in the radiative transfer simulations. Due to its simplicity and efficiency, the H-G phase function is widely used in the IR radiative transfer calculations as an approximation for describing the phase function of cloud particles. In this section we compare the H-G phase function with more realistic phase function calculated for hexagonal ice crystals from the FDTD and an improved geometric optics methods. The phase functions for individual crystals are averaged over the 34 ice cloud size distributions as discussed previously. For two different size distributions, Fig.5 shows a comparison between the actual phase functions derived for hexagonal ice crystals and the H-G phase functions derived using the asymmetry factor obtained for each distribution. Compared with the nonspherical ice crystal phase functions, the H-G phase function is smoother and smaller in magnitude in both the forward- and back-scattering directions.

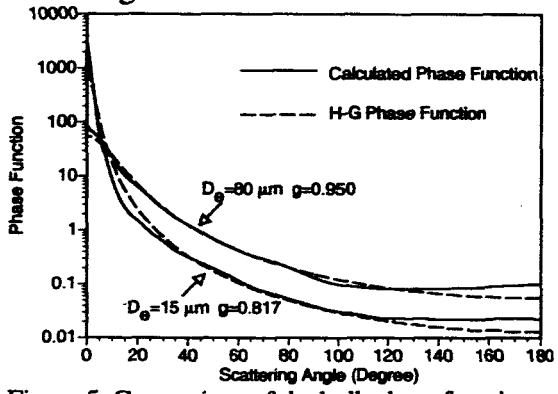

Figure 5. Comparison of the bulk phase function calculated using nonspherical ice habits (droxtals and hexagonal columns) with a Henyey-Greenstein phase function for two effective particle sizes.

Figure 6 shows the differences in the simulated spectral brightness temperatures (converted from the upward spectral flux) at the aircraft level (20 km) between the results derived using the actual phase function derived for nonspherical crystals and the simplified H-G phase function. The brightness temperature using the derived phase function is a little greater than that of the H-G phase function in most cases. This is due to the fact that the forward scattering of derived phase function is usually larger than that of the H-G phase function. The largest differences occur at wavenumbers where strong scattering occurs (1000–1300 cm^{-1}) for large particle effective sizes. For small particles, the difference between the two phase functions is much less, with brightness temperatures generally differing by less than 0.4 K. This may be due to the offset of the difference phase functions within 0-90°. For clouds containing larger ice crystals with a large value of the asymmetry factor, the brightness temperature difference can be more than 1 K. The modified the H-G phase function, such as the double H-G phase function, may offer a better result.

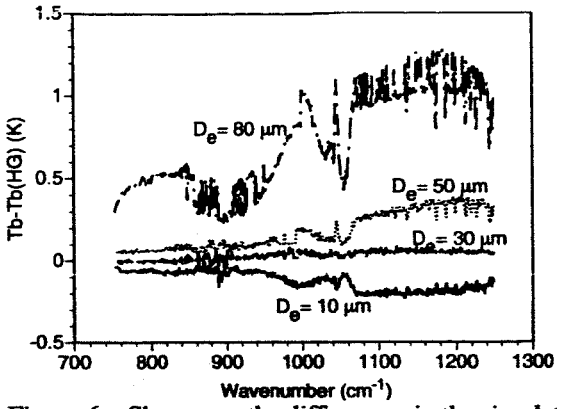

Figure 6. Shown are the differences in the simulated spectral brightness temperatures from use of the actual phase function derived for nonspherical crystals and the simplified H-G phase function in the radiative transfer calculations. Results are shown for simulations of clouds having four effective particle sizes (10, 30, 50, and 80 μm). The calculations are performed at the aircraft altitude (20 km) and assume the US standard atmospheric model; a surface skin temperature of Ts=288.1K; a cloud altitude of 10 km, and an optical thickness τ=1.

Sensitivity study and error analysis

In this section we present the physical basis of the retrieval technique by investigating the sensitivity of high spectral resolution IR brightness temperatures to the effective particle size and optical thickness. As this knowledge will later be used to derive the cloud properties from HIS radiances, we have used an observer altitude of 20 km, the cruising altitude of the ER-2 aircraft, in the upwelling radiance calculations. We also investigate the influence of the atmospheric profiles and the inaccuracies in the cloud temperature and surface skin temperature on the retrieval results.

3.1 Sensitivity of IR Radiance to Effective Particle Size

Figure 7 illustrates the sensitivity of the upwelling brightness temperature spectrum to the ice cloud effective particle size. The spectral brightness temperatures between atmospheric molecular absorption lines (i.e., the atmospheric windows) increase with wavenumber within the 760–1000cm^{-1} region because the absorption of ice crystal particles decreases with wavenumber and the absorption is also size-dependent. The cirrus clouds with smaller effective sizes absorb more radiance underneath in the region of small wavenumbers, leading to a steeper slope for cirrus clouds composed of small particles than for cirrus clouds composed of large particles.

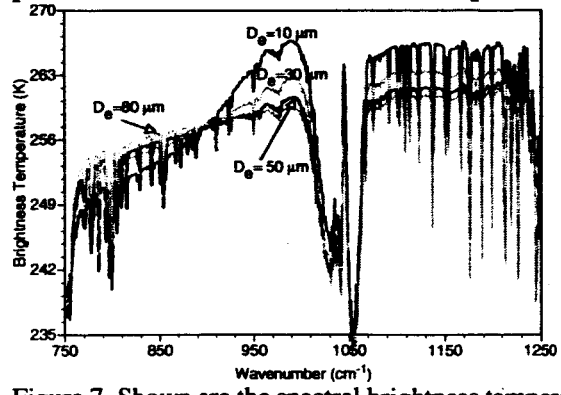

Figure 7. Shown are the spectral brightness temperatures at the aircraft level (20km) as a function of wavenumber for four effective particle sizes (10, 30, 50, and 80 μm). The calculations assume the US standard atmospheric model, a surface skin temperature of 288.1 K, a cloud altitude of 10 km, and an optical thickness τ=1.

From the brightness temperature at atmospheric window wavenumbers, ignoring the strong absorption wavenumbers to remove the absorption lines between 790–960 cm^{-1} and interpolating the brightness temperatures across the gaps, we notice that there is a marked sensitivity in the slope of the observed brightness temperature to the effective particle size (see Fig.8). This sensitivity, in which the slope in brightness temperature increases with decreasing particle size, forms the basis for the inference of effective particle size. We calculate the brightness temperature at the atmospheric windows in the 790–960 cm^{-1} region, and obtain the slope for a range of different effective particle sizes and values of optical thickness.

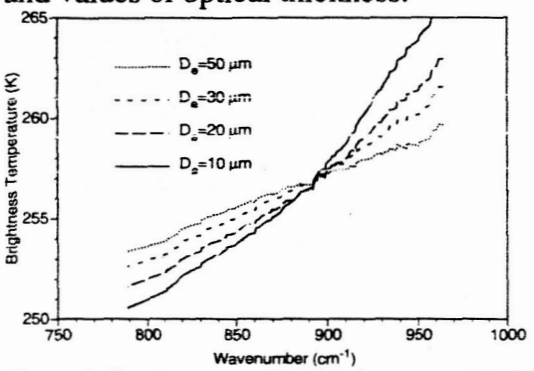

Figure 8. For the spectral region between 790–960 cm^{-1}, the absorption lines between 790–960 cm^{-1} are removed and the resulting window brightness temperatures are interpolated across the gaps. This process more clearly shows how the slope of the observed spectral brightness temperature, with respect to wavenumber, depends upon the effective particle size.

As shown in Fig. 9, the variation of the slope is most sensitive to particle size for small particles and optical thicknesses between 0.4 and 4. For example, for a cloud having an optical thickness of 1, the slope decreases from 9 K/μm to 2 K/μm as the effective particle size increases from 10 μm to 80 μm.

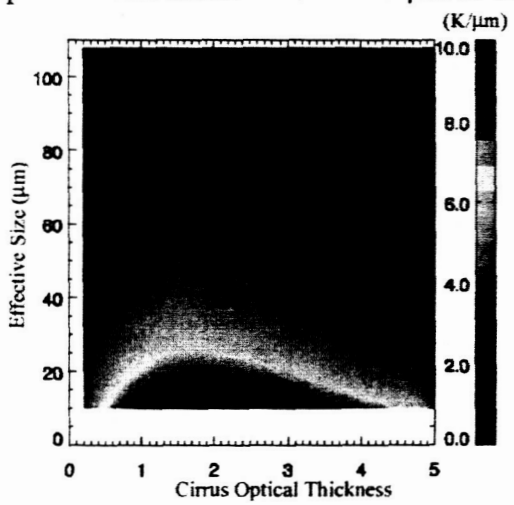

Figure 9. As in Fig. 8, but extended to include both the effect of optical thickness and particle size on the slope of the spectral brightness temperatures and wavenumber between 790–960 cm^{-1}.

3.2 Sensitivity of IR Radiance to Optical Thickness of Clouds

Figure 10 shows simulated upwelling brightness temperature at a 20-km altitude for four values of optical thickness and a fixed effective particle size of 30 μm. The brightness temperature varies with wavenumber between 750–1000 cm^{-1} for small to moderate

optical thicknesses. As shown in Fig. 10, the brightness temperature decreases more than 40 K as the optical thickness increases from 0.5 to 5. For optically thick ice clouds (optical thickness larger than 5), the brightness temperature has less dependence on wavenumber.

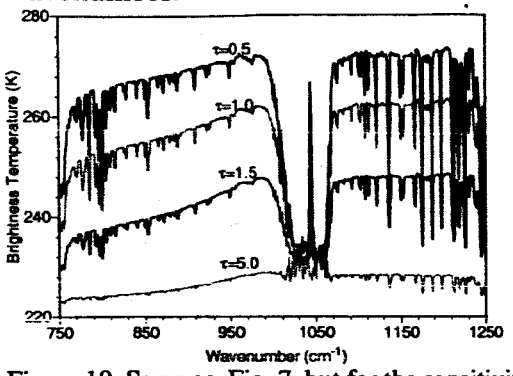

Figure 10. Same as Fig. 7, but for the sensitivity of spectral brightness temperature to the cloud optical thickness. The assumed effective particle size is fixed at 30 μm.

3.3. Error Analysis

The brightness temperature discretization in Fig. 9 is 0.5 K/μm. If we assume the minimum measurable temperature difference is 1 K then the effective particle size cannot be accurately retrieved if the variation of brightness temperature difference between 950 and 790 cm^{-1} is less than 1 K due to the variation of the effective particle size. Further theoretical error analysis suggested that, for a threshold of 0.5 K/μm, the maximum retrievable effective size is no larger than 80 μm with an uncertainty of 10 μm. The uncertainty decreases to about 2 μm when the effective size is 10 μm. Similarly, the maximum retrievable optical thickness is approximately 8 with an uncertainty of 1. For the case of a visible optical thickness of 1, the uncertainty decreases to less than 0.1.
In the IR spectrum, the surface skin temperature, cloud temperature and atmospheric profile contributed significantly to the top of atmosphere radiance. Hence, in the remains of the section, we study the effects of uncertainties in surface and cloud temperature to retrieval results. We also investigate the variation of the sensitivity for different atmospheric profiles.

3.4 Effects of Surface and Cloud Temperature on Retrieval Accuracy

In this section we analyze the effects of inaccurate surface and cloud temperature that are provided as inputs to the algorithm, on the accuracy of the inferred microphysical and optical properties. Cloud-top pressure or temperature may be inferred by methods such as the CO_2 slicing method [48] or by the minimum local emissivity variance (MLEV) method [49]. The MLEV algorithm uses a physical approach in which the local spectral variances of cloud emissivity are calculated for a number of assumed cloud pressures. The optimal cloud emissivity spectrum is that which has the minimum local emissivity variance among the retrieved emissivity spectra associated with different assumed cloud pressures. This technique is based on the observation that the absorption, reflection, and scattering processes of clouds exhibit relatively limited localized spectral emissivity structure in the 750–1250 cm^{-1} spectral region. Any retrieved cloud emissivity that exhibits spectral variation similar to that of carbon dioxide and water vapor absorption is indicative of an incorrect specification of cloud pressure level and its associated spectral emissivity. MLEV analysis shows that cloud pressure root mean square errors for a single

layer cloud with effective cloud emissivity greater than 0.1 are ~30 hPa, ~10 hPa, and ~50 hPa, for high, middle, and low clouds, respectively.

Errors in the assigned cloud pressure and its corresponding temperature will affect the retrieval of optical thickness. Figure 11 shows the predicted error in the retrieved optical thickness as a function of cloud temperature error. The error of cloud temperature is assumed to be within ±7 K, corresponding to the variation of temperature at a cloud altitude of 10±1 km. A lower-than-actual cloud temperature will result in an overestimate of the optical thickness, while a higher-than-actual cloud temperature will lead to an underestimate of optical thickness. The impact of the cloud temperature error is more pronounced for optically thick ice clouds than for optically thin ice clouds. Generally, the error in the retrieved optical thickness is less than 10% if the cloud temperature is within ±5 K of the true temperature and the cloud optical thickness is less than 2.

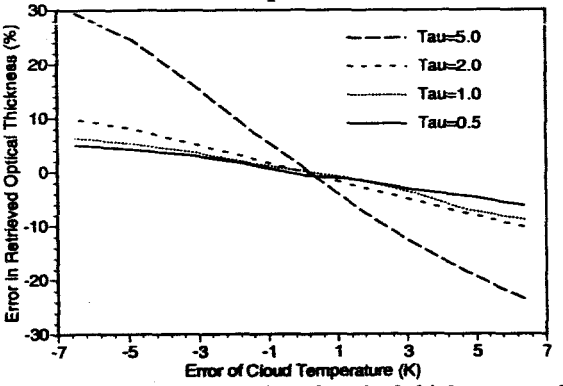

Figure 11. Errors in retrieved optical thickness resulting from an error in cloud temperature for four optical thicknesses. The ice cloud has an effective particle size of 25 μm. The actual cloud temperature is assumed to be 223.3 K, but varies from 229.7 to 216.8 K.

Figure 12 shows the relationship between the retrieved effective particle size and the cloud temperature error. Different cloud temperatures result in different brightness temperature slopes, and thus lead to effective particle size retrieval errors. The error is within ±15% if the cloud temperature error is within ±5 K.

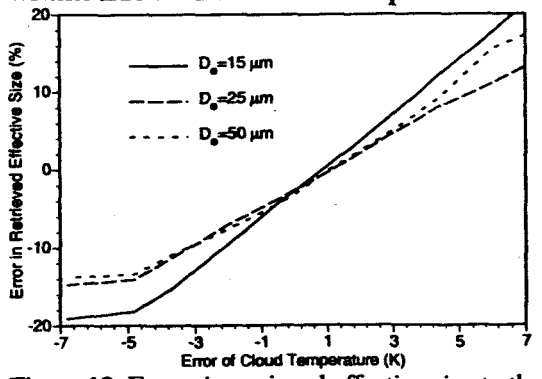

Figure 12. Errors in retrieved effective size to the error of cloud temperature for 3 effective particle sizes. The ice cloud has an optical thickness of 1.

Figure 13 shows the error in retrieved optical thickness as a function of surface skin temperature error. An error in the surface skin temperature has a pronounced influence on the retrieval of optical thickness if the cloud is optically thin, because the upwelling radiation is primarily from the surface, with some modest attenuation by the atmosphere and cloud. For very thick clouds, an error in the surface skin temperature has little influence on the retrieved optical thickness. For the retrieval accuracy of optical

thickness (Fig. 13) to be better than 10%, the surface skin temperature error should be less than ±2.5 K.

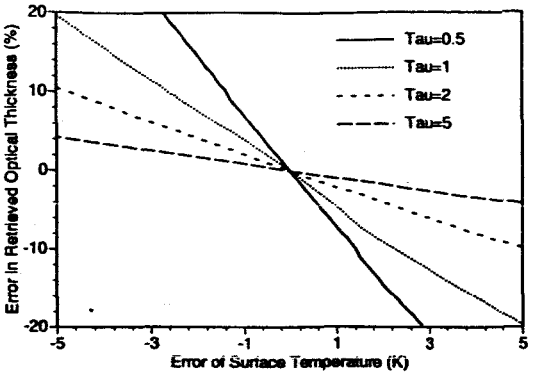

Figure 13. Errors in retrieved optical thickness resulting from an error in surface skin temperature for four cloud optical thicknesses. The ice cloud has an effective particle size of 25 μm and is located at an altitude of 10 km.

Figure 14 shows the dependence of the retrieved error in effective particle size on the error in surface skin temperature. Compared to the results in Fig. 13, an error in surface skin temperature (Fig. 14) has less influence on the effective particle size than on the optical thickness, because the variation of the surface skin temperature does not change as much with the slope of brightness temperature between 790–960cm^{-1}. If the error of surface skin temperature is within ±2.5 K, the error of retrieved effective particle size will be within ±5%.

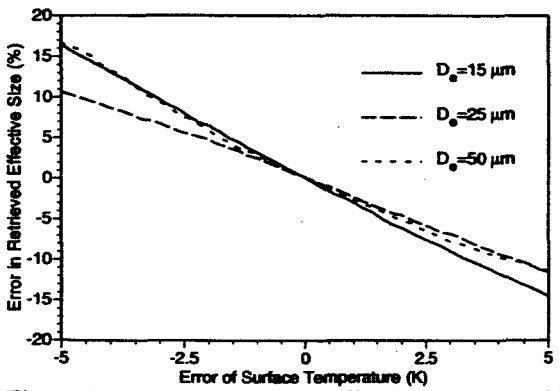

Figure 14. Errors in retrieved effective size caused by an error in surface skin temperature for three effective particle sizes. The cloud optical thickness is constant at 1, and the cloud altitude is 10 km.

3.5 Effect of the Atmospheric Profiles

We now investigate the sensitivity of the brightness temperature to different regional average atmospheric profiles by calculating the brightness temperature difference between clear-sky and cloudy radiance, defined as the cloud forcing. Figure 15 shows the cloud forcing for both a climatological tropical (TRO) and subarctic winter (AW) atmosphere for two assumed values of cloud optical thickness. We assume the surface skin temperature is the same as the atmospheric temperature of the lowest layer, that is, 300 K (tropical) and 257.1 K (subartic winter). Because the upwelling brightness temperature for the subarctic winter atmosphere is much lower than that of the tropical atmosphere, the sensitivity decreases for the subarctic winter atmosphere relative to a warmer tropical atmosphere (I'm not sure I agree with this – is not just a result of the

temperature of the cloud and the temperature of the surface/atmosphere are more similar in the artic case?). Even for the subartic winter atmopsheric model, however, the variation of cloud forcing can still be more than 20 K when the optical thickness increases from 0.5 to 2. Thus, the IR spectra still contains sufficient information in these conditions from which the properties of ice clouds can be inferred using the simultaneous retrieval technique.

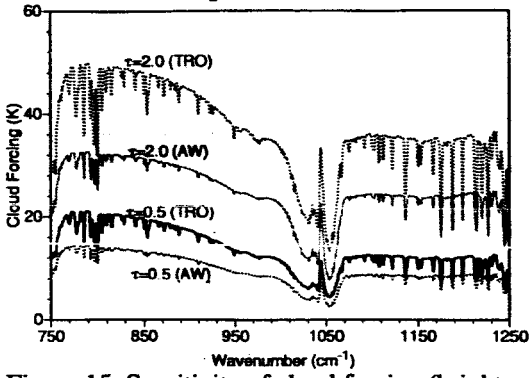

Figure 15. Sensitivity of cloud forcing (brightness temperature difference between clear and cloudy sky) to the atmospheric model for two cloud optical thicknesses.

4. Inference of Ice Cloud Microphysical and Optical Properties

4.1 Simultaneous Retrieval Algorithm

An understanding of the above dependence of the upwelling radiance to cloud properties leads us to the following methodology for simultaneous retrieval of effective particle size and optical thickness. First, the clear-sky atmospheric optical thickness profile is calculated with the LBL radiative transfer code. Given an ice cloud height and temperature, a series of spectral radiances are simulated using DISORT for a range of cloud effective particle sizes and optical thicknesses, and additional pre-calculated cloud optical properties discussed in Section 2.1. By matching the slope of brightness temperature in the 790–960 cm^{-1} band to the observed spectrum, the effective particle size of the ice cloud D_e can be estimated (note that, at this initial stage, a first-guess optical thickness τ is used). Then the optical thickness is derived by comparing the observed spectrum to the simulations in 1100–1250 cm^{-1} band with the values of D_e determined in the previous step. The final particle size and optical thickness are obtained by iteration until the differences are minimized between the observed and simulated IR spectrum. A best-fit value is reached when the difference (variance) between the observed and simulated IR spectrum within the two bands is minimal.

In the following section, we apply the simultaneous retrieval algorithm outlined above to HIS data collected from two field experiments.

4.2 Case study 1: FIRE-ACE Experiment

During FIRE-ACE [50], upwelling spectral radiance was observed by the HIS instrument onboard the ER-2 aircraft from an altitude of 20 km. HIS data from Band 1 (750–1080 cm^{-1}) and Band 2 (1100–1250 cm^{-1}) were selected for analysis between 2345 UT and 0020 UT on 22–23 May 1998. This period provides example observations for water clouds (before 0007 UT), clear sky (0007 to 0010 UT), and high ice clouds (after 0010 UT). The data were recorded in Alaska near 67.52°N, 150.60°W. Figure 16 shows the Cloud Lidar System (CLS) imagery for this period which provides information on the cloud-top altitude [51] and was used together with a MODIS Airborne Simulator (MAS)

image (not shown here) to discriminate between clear sky, water cloud and ice cloud conditions.

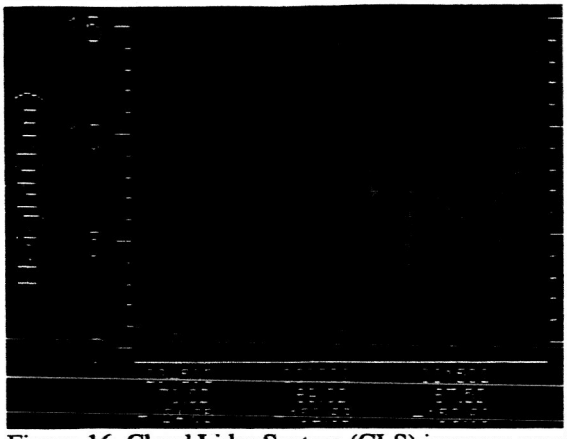

Figure 16. Cloud Lidar System (CLS) imagery providing information on cloud heights and boundaries. The scanning times, given in the format HH:MM:SS, used in this paper are 00:05:23 for the water cloud data, and 00:17:01 for ice cloud data. Scanning locations in degrees latitude and longitude are given below the time values.

The HIS brightness temperature spectrum for clear sky (0009 UT) is shown in Fig. 17, while those for water clouds (0005 UT) and high ice clouds (0017 UT) are shown in Fig. 18. Also plotted on these two figures are the best-fit simulated radiances that were generated from temperature, pressure and relative humidity data from a nearby rawinsonde at 2324 UT on May 22 1998, together with cloud properties determined using our retrieval technique. It should be pointed that the atmospheric parameters, particular the surface skin temperature and cloud temperature, are important to the retrieval as studied in previous section. The *in-situ* real time temperature profile should be used for the retrieval if possible.

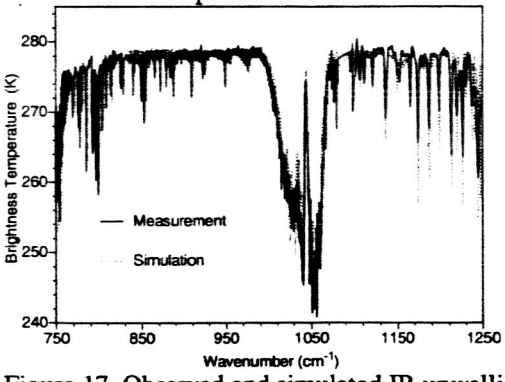

Figure 17. Observed and simulated IR upwelling spectra under clear-sky conditions for 23 May 1998, 00:09:04 UT; surface skin temperature is 279 K.

Fig. 18 demonstrates that the observed spectral signature of the ice cloud is quite different from that of the water cloud. The brightness temperature of the ice cloud increases with wavenumber over the 750–1000cm^{-1} region. This expected result, as previously mentioned, is due to the spectral variation of the absorption of ice crystals.

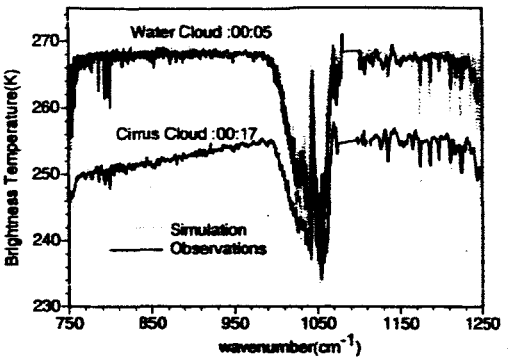

Figure 18. The observed and simulated upwelling IR spectra for ice and water cloud conditions (the number in the figure is given in the format HH:MM UT on May 23 1998).

Fig. 19 illustrates the process of matching the simulated and observed brightness temperatures by varying (and thus, when the brightness temperatures match, retrieving) the cloud properties in the simulations. The left panel of Fig.19 shows comparisons of the observed HIS spectrum (solid black curve) with simulated brightness temperatures for a number of trial effective particle sizes D_e=35, 45, and 60 μm and a first-guess optical thickness τ =1.43, within the 760–1000 cm^{-1} band. The right panel of Fig.19 shows brightness temperatures for the best-matched effective particle size D_e=45.0 μm (as determined from the previous step as illustrated in left panel of Fig.19) with trial optical thickness values τ =1.2, 1.43, and 1.6 within the 1100–1250 cm^{-1} band). The effective cloud particle size is retrieved by fitting a line between 790–960 cm^{-1}. The resultant values of the effective particle size and optical thickness in this case are therefore 45 μm and 1.43 respectively.

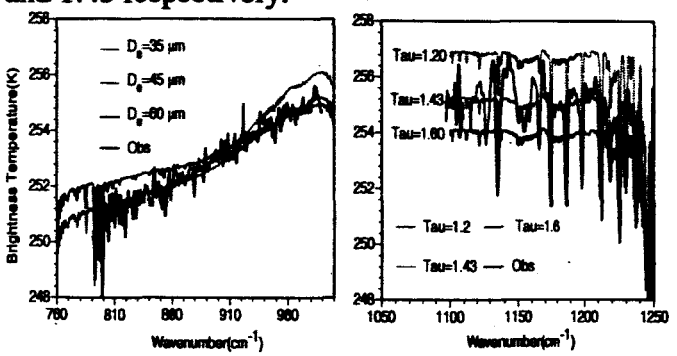

Figure 19. The simultaneous retrieval of the effective size and optical thickness of ice clouds from HIS spectra. (a) Brightness temperature versus particle size assuming τ=1.43. (b) Brightness temperature versus optical thickness assuming D_e=45 μm. Date: 23 May 1998, 00:17:01 UT. The surface skin temperature is 267.6 K, and the cloud altitude is 7.0 km.

4.3 Case Study 2: SUCCESS Experiment (small particle case)

Smith et al. [2] reported a strong absorption signature of very small cirrus cloud particles during SUCCESS in 1996. Figure 20 shows the HIS spectrum collected from the ER-2 during an overflight of a jet aircraft contrail, which generally consists of very small particles. The best-fit simulated spectral brightness temperatures, also plotted, are simulations for an ice cloud model based solely on droxtals with an effective particle size of 12.5 μm, and an optical thickness of 1.60. The simulation generally agrees well with the observed spectrum (except at 990 cm^{-1}, probably due to the residual effect of an imperfect ozone concentration profile) and indicates that the droxtal crystal habit seems to be a realistic approximation for small ice particles. *Chung et al.* [14] calculated the

spectrum for this case by assuming that ice clouds are composed of spherical ice particles with an assumed Gamma size distribution. The retrieved effective radius (7.35 μm) and IWP (6.85 g/m^2) is equivalent to an optical thickness of 1.5. Our retrieved optical thickness is close to Chung's result, but the effective particle size is a little smaller. The differences are due to the more complex ice habit (droxtal) used in our study. A droxtal with the same maximum dimension will have smaller effective size than the ice sphere. Thus, the retrieved effective size is a little small by assuming the droxtal instead of sphere. The effect of ice crystal nonsphericity deserves a further study.

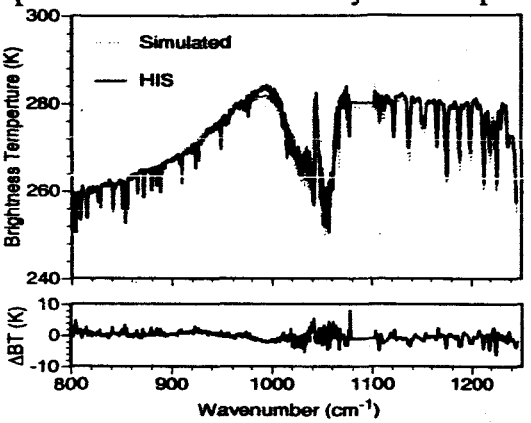

Figure 20. The comparison of observed and simulated upwelling IR spectra at 20 km altitude for a jet contrail composed of primarily small ice particles (D_e=12.5 μm, τ =1.6).

5. Summary

Within the 750–1000 cm^{-1} spectral region, the slope of brightness temperature is sensitive to ice crystal effective particle size, particularly for small particles. At wavenumbers between 1100 and 1250 cm^{-1}, the spectrum is more sensitive to the optical thickness than to particle size. Thus, using the terrestrial window information within the 750–1250 cm^{-1} spectral band, we can infer the optical thickness and effective particle size for ice clouds simultaneously.

While the error analysis shows that the uncertainty of the retrieved optical thickness and effective particle size exhibits a small variation. The error for retrieving particle size in conjunction with an uncertainty of 5 K in cloud temperature, or a surface temperature uncertainty of 2.5 K, is less than 15%. The corresponding error in the uncertainty of optical thickness is within 5-20%, depending on the value of cloud optical thickness. The maximum effective particle size that may be retrieved with the present approach (i.e., an upper limit) is 80 μm with an uncertainty of approximately 10 μm at D_e=80 μm, and about 2 μm uncertainty at D_e=10 μm. The maximum retrievable optical thickness is approximately 8 with an uncertainty of 1. For the case of optical thickness 1, the uncertainty decreases to less than 0.1.

The applicability of the technique is demonstrated using the aircraft–based HIS data from the SUCCESS in 1996 and FIRE-ACE in 1998. Both larger (45 μm) and smaller (12.5 μm) effective particle sizes simultaneous retrievals yield reasonable fit to the observed spectra. Spectral temperature differences of ~4 degree and >20 degree Kevin (the slope of the spectral brightness temperatures and wavenumber between 790–960 cm^{-1}) further demonstrate the forward modeling of cloudy measurements and retrieval algorithm is capability of obtaining reliable cloud property. Subsequent cloud modeling study and retrieval analysis verification using space-borne and active cloud measurements, and *in-situ* measurements will be conducted to advance our ability to refine this technique.

Acknowledgments
This study is supported by the GIFTS-IOMI MURI project. P. Yang's effort involved here also supported by research grants (NAG-1-02002, NAG5-11374) from the NASA Radiation Sciences Program managed by Dr. Donald Anderson and National Science Foundation (NSF) CAREER Award (ATM-0239605).

References

[1] D. K. Lynch, K. Sassen, D. O. Starr and G. Stephens (Eds.), Cirrus, (Oxford Univ. Press, New York, 2002)

[2] W. L. Smith, S. Ackerman, H. Revercomb, H. Huang, D. H. DeSlover, W. Feltz, L. Gumley and A. Collard, "Infrared spectral absorption of nearly invisible cirrus clouds," *Geophys. Res. Lett.*, VOL. 25, pp.1137–1140, 1998.

[3] G. L. Stephens,S.C. Tsay, P.W. Flatau, "The relevance of microphysical and radiative properties of cirrus clouds to climate and clime feedback," *J. Atmos. Sci.*, vol. 47, pp.1742-1753,1990.

[4] K. N. Liou, "Influence of cirrus clouds on weather and climate processes: A global perspective," *Mon. Wea. Rev.*, vol. 114, pp.1167-1199,1986.

[5] T. Nakajima and M. D. King, "Determination of the Optical Thickness and Effective Particle Radius of Clouds from Reflected Solar Radiation Measurements. Part I: Theory," *J. Atmos. Sci*, vol.47, pp. *1878-1893*,1990.

[6] M. D. King, W. P. Menzel, Y. J. Kaufman, D. Tanré, B. C. Gao, S. Platnick, S. A. Ackerman, L. A. Remer, R. Pincus, and P. A. Hubanks, "Cloud and Aerosol Properties, Precipitable Water, and Profiles of Temperature and Humidity from MODIS," *IEEE Trans. Geosci. Remote Sens.*, vol.41, pp.442-458, 2003.

[7] S. Platnick, M.D. King, S. A. Ackerman, W. P. Menzel, B.A. Baum, J. C. Riédi, and R. A. Frey, "The MODIS Cloud Products: Algorithms and Examples from Terra. IEEE Transactions on Geoscience and Remote Sensing," *IEEE Trans. Geosci. Remote Sens.*, vol.41, pp.459-473, 2003.

[8] C.J. Stubenrauch, R. Holz, A. Chedin, D.L. Mitchell, A.J. Baran, "Retrieval of cirrus ice crystal sizes from 8.3 and 11.1μm emissivities determined by the improved initialization inversion of TIROS-N operational vertical sounder observations," *J Geophys Res* , vol.104, pp.793–808,1999.

[9] P. Zuidema, "Convective Clouds over the Bay of Bengal," *Mon. Wea. Rev.*, vol.131, pp. 780-798, 2003.

[10] Smith, W. L., D. K. Zhou, F. W. Harrison, H. E. Revercomb, A. M. Larar, H.-L. Huang, and B. Huang, 2000: Hyperspectral remote sensing of atmospheric profiles from satellites and aircraft, Proceedings of SPIE, William L. Smith and Yoshifumi Yasuoka, editors. *Hyperspectral Remote Sensing of the Land and Atmosphere*. 9-12 Oct. 2000, 94-102.

[11] Huang, H.-L., H. E. Revercomb, J. Thom, P. B. Antonelli, B. Osborne, D. Tobin, R. Knuteson, R. Garcia, S. Dutcher, J. Li, and W. L. Smith, 2000: Geostationary Imaging FTS (GIFTS) Data Processing: Measurement Simulation and Compression. Proceedings of SPIE, William L. Smith and Yoshifumi Yasuoka, editors. *Hyperspectral Remote Sensing of the Land and Atmosphere*. 9-12 Oct. 2000, 103-114.[12] Glumb R. J., D. C. Jordan, P. Mantica, 2002: Development of the Crosstrack Infrared Sounder (CrIS) sensor design. Proceedings of SPIE, Infrared Spaceborne Remote Sensing IX; Marija Strojnik, Bjorn F. Andresen; Editors. Proc. SPIE Vol. 4486, p. 411-424.

[13] S. Ou, K. N. Liou, P. Yang, P. Rolland, T. R. Caudill, J. Lisowski, and B. Morrison, " Airborne retrieval of cirrus cloud optical and microphysical properties using ARES 5.1-5.3μm channel data," *J. Geophys. Res.*, vol.103, pp.23231-23242,1998

[14]S. Chung, S. Ackerman, P. F. Van Delst, and W. P. Menzel, "Model calculations and interferometer measurements of ice-clouds characteristics," *J. Appl. Meteor.*, vol. *39*, pp.634–644, 2000.

[15]S. A. Ackerman, W. L. Smith, J. D. Spinhirne, and H. E. Revercomb, "The 27-28 October 1986 FIRE IFO cirrus case study: Spectral properties of cirrus clouds in the 8-12 μm window," *Mon. Wea. Rev.*, vol.118, pp.2377-2388, 1990.

[16]R.J. Bantges, J. E. Russell, and J. D. Haigh, "Cirrus cloud top-of-atmosphere radiance spectra in the thermal infrared," *J. Quant. Spectrosc. Radiat. Transfer*, vol.63, pp. 487–498, 1999.

[17] D. H. DeSlover, W. L. Smith, P. K. Piironen, and E. W. Eloranta, "A methodology for measuring cirrus cloud visible-to-infrared spectral optical thickness ratios," *J. Atmos. Oceanic Technol.*, vol.16, pp.251–262, 1999.

[18] B.H.K. Kahn, A. Eldering, F. W. Irion, F. P. Mills, B. Sen, and M. R. Gunson, "Cloud identification in Atmospheric Trace Molecule Spectroscopy infrared occultation measurements," *Appl. Opt.*, vol. 41, pp.2768–2780, 2002.

[19] A. Eldering, F. W. Irion, A. Y. Chang, M. R. Gunson, F. P. Mills, and H. M. Steele, "Vertical profiles of aerosol volume from high-spectral-resolution infrared transmission measurements," I. Methodology, *Appl. Opt.*, vol. 40, pp.3082–3090, 2001.

[20]C. Rathke and J. Fischer, "Retrieval of cloud microphysical properties from thermal infrared observations by a fast iterative radiance fitting method," *J. Atmos. Oceanic Technol.*, vol. 17, pp.1509–1524, 2000.

[21]M.D. Chou, K.T. Lee, S. C. Tsay, and Q. Fu, "Parameterization for cloud longwave scattering for use in atmospheric models," *J. Climate*, vol.12, pp.159-169,1999.

[22] A. J. Heymsfield and C. M. R. Platt, "A parameterization of the particle size spectrum of ice clouds in terms of the ambient temperature and the ice water content," *J. Atmos. Sci.*, vol.41, pp.846–855, 1984.

[23] A. J. Heymsfield and J. Iaquinta, "Cirrus crystal terminal velocities," *J. Atmos. Sci.*, vol.5, pp.916–938, 2000.

[24] P. Yang, B. A. Baum, A. J. Heymsfield, Y. X. Hu, H.-L. Huang, S.-Chee Tsay, and S. Ackerman, "Single-scattering properties of droxtals," *J. Quant. Spectrosc. Radiat. Transfer.* vol. 79–80, pp.1159–1169, 2003.

[25] P. Yang, B. C. Gao, B. A. Baum, Y. X. Hu, W. J. Wiscombe, S. C. Tsay, D. M. Winker, and S. L. Nasiri, "Radiative properties of cirrus clouds in the infrared (8–13 μm) spectral region," *J. Quant. Spectrosc. Radiat. Transfer*, vol.70, pp.473–504, 2001.

[26].P. Yang, and K. N. Liou, "Finite-difference time domain method for light scattering by small ice crystals in three-dimensional space," *J. Opt. Soc. Amer.*, vol. A13, pp. 2072-2085, 1996.

[27] W. J. Wiscombe, "Improved Mie scattering algorithms," *Appl. Opt.*, vol.*19*, pp.1505–1509, 1980.

[28]Q. Fu, W.B. Sun, P.Yang, "On modeling of scattering and absorption by cirrus nonspherical ice particles at thermal infrared wavelengths," *J. Atmos Sci,* vol.56, pp.2937–2947,1999.

[29] P. Yang and K. N. Liou, "Geometric-Optics-integral-equation method for light scattering by nonspherical ice crystals," *Appl. Opt.*, vol.35, pp.6568-6584,1996

[30] P. Yang, B.-C. Gao, B. A. Baum, W. Wiscombe, M. I. Mischenko, D. M. Winker, and S. L. Nasiri, Asymptotic solutions of optical properties of large particles with strong absorption. *Appl. Opt.*, vol.40, pp.1532-1547, 2001

[31] Y.K. Lee, P. Yang, M.I. Mishchenko, B. A. Baum, Y. Hu, H.-L. Huang, W.J. Wiscombe, and A. J. Baran, "On the use of circular cylinders as surrogates for hexagonal pristine ice crystals in scattering calculations at infrared wavelengths," *Appl. Opt.* vol.42, pp. 2653-266,2003

[32] M. I. Mishchenko and L. D. Travis, Capabilities and limitations of a current FORTRAN implementation of the T-matrix method for randomly oriented rotationally symmetric scatters, *J. Quant. Spectrosc. Radiat. Transfer*, 60, 309-324, 1998.

[33] Q. Fu, P. Yang and W. B. Sun, "An accurate parameterization of the infrared radiative properties of cirrus clouds for climate models," *J. Climate*, vol.25, pp.2223–2237, 1998.

[34] D.L.Mitchell, S.K.Chai, Y.Liu, A.J.Heymsfeld, Y.Dong, "Modeling cirrus clouds. PartI: treatment of bimodal size spectra and case study analysis," *J. Atmos. Sci.* vol.53, pp.2952 –2966,1996.

[35]. Q. Fu and W. B. Sun, "Retrieval of cirrus particle sizes using a split-window technique: a sensitivity study, " *J. Quant. Spectrosc. Radiat. Transfer*, vol. 70, pp.725–736, 2001.

[36] W. P. Arnott, Y. Y. Dong , and J. Hallett, "Extinction efficiency in the infrared (2-18 μm) of laboratory ice clouds: observations of scattering minimum in the Christiansen bands of ice," *Appl. Opt.* , vol.34, pp.541–551, 1995.

[37] P. Yang, K. N. Liou and W. P. Arnott, "Extinction efficiency and single-scatttering albedo for laboratory and natural cirrus clouds," *J. Geophys. Res.*, vol. 103, pp.825–835, 1997.

[38] J.E. Hansen and L.D. Travis, "Light scattering in planetary atmospheres," Space Sci. Rev., vol.16,pp527-610,1974.

[39] M.D. Chou, and L. Kouvaris, "Monochromatic calculations of atmospheric radiative transfer due to molecular line absorption," *J. Geophys. Res.*,vol. 91, pp.4047-4055, 1986.

[40] L. S. Rothman, C. P. Rinsland, A. Goldman et al., "The HITRAN Molecular Spectroscopic Database and HAWKS (HITRAN Atmospheric Workstation): 1996 Edition," *J. Quant. Spectrosc. Radiat. Transfer*, vol. 60, pp. 665–710, 1998.

[41] J. F. Kielkopf, "New Approximation to the Voigt Function with application to spectral line profiles," *J. Opt. Sci. Am.*, vol. 63, pp.987–995, 1973.

[42] D. C. Tobin, F. A. Best, S. A. Clough, R. G. Dedecker, R. G. Ellingson, R. K. Garcia, H. B. Howell, R. O. Knuteson, E. J. Mlawer, H. E. Revercomb, J. J. Short, P. F. W. van Delst, and V. P. Walden, "Downwelling spectral radiance observations at the SHEBA ice station: Water vapor continuum measurements from 17–26 μm, " *J. Geophys. Res.*, vol. 104, pp.2081–2092, 1999.

[43] K. Stamnes, S. C. Tsay, W. Wiscombe and K. Jayaweera, "A numerically stable algorithm for discrete-ordinate-method radiative transfer in multiple scattering and emitting layered media," *Appl. Opt.*, vol. 27, pp.2502–2509, 1988.

[44].Y. X. Hu, B Wielicki, B. Lin, G. Gibson, S. C. Tsay, K. Stamnes, and T. Wong, "Delta-fit: A fast and accurate treatment of particle scattering phase functions with weighted singular-value decomposition least-square fitting," J. Quant. Spectrosc. Radiat. Transfer, vol. 65, pp.681-690, 2000.

[45] M.I. Mishchenko, J. W. Hovenier, and L. D. Travis (Eds.), *Light Scattering by Nonspherical Particles: Theory, Measurements, and Applications*, San Diego, Academic Press, 2000.

[46] M. I. Mishchenko, W. B. Rossow, A. Macke, and A. A. Lacis, "Sensitivity of cirrus cloud albedo, bidirectional reflectance, and optical thickness retrieval to ice-particle shape," *J. Geophys. Res.*, vol.101, pp.16973-16985,1996.

[47] Y. Takano, K. N. Liou, and P. Minnis, "The effects of small ice crystals on cirrus infrared radiative properties," *J. Atmos. Sci.*, vol.49, pp.1487-1493,1992

[48] D. P. Wylie and W. P. Menzel, "Eight years of global high cloud statistics using HIRS," *J. Climate*, vol. 12, pp.170–184,1999.

[49] H. L. Huang, W. L. Smith, J. Li, P. Antonelli, X. Wu, R. O. Knuteson, B. Huang, and B. J. Osborne, "Minimum local emissivity variance retrieval of cloud altitude and effective spectral emissivity simulation and initial verification," accepted by *J. Appl. Meteo.*, 2003.

[50] J. A. Curry, P. V. Hobbs, M. D. King, D. A. Randall, P. Minnis, G. A. Isaac, J. O. Pinto, T. Uttal, A. Bucholtz, D. G. Cripe, H. Gerber, C. W. Fairall, T. J. Garrett, J. Hudson, J. M. Intrieri, C. Jakob, T. Jensen, P. Lawson, D. Marcotte, L. Nguyen, P. Pilewskie, A. Rangno, D. C. Rogers, K. B. Strawbridge, F. P. J. Valero,.A. G. Williams, and D. Wylie, "FIRE Arctic Clouds Experiment," *Bull. Amer. Meteor. Soc.*,vol.81, pp.5–29, 2000.

[51] J. D. Spinhirne and W. D. Hart, "Cirrus structure and radiative parameters from airborne lidar and spectral radiometer observations," *Mon. Wea. Rev.*, vol.118, pp.2329–2343, 1990.